molecules

MDPI

Article

Luminous Self-Assembled Fibers of Azopyridines and Quantum Dots Enabled by Synergy of Halogen Bond and Alkyl Chain Interactions

Ying Pan [1,†], Lulu Xue [1,†], Yinjie Chen [1,*], Yingjie Hu [2,*], Zhicheng Sun [1], Lixin Mo [1], Luhai Li [1,*] and Haifeng Yu [3]

[1] Beijing Engineering Research Center of Printed Electronics Institution, Beijing Institute of Graphic Communication, Beijing 102600, China
[2] Nanjing Key Laboratory of Advanced Functional Materials, Nanjing Xiaozhuang University, Nanjing 211171, China
[3] School of Materials Science and Engineering, Peking University, Beijing 100871, China
* Correspondence: chenyinjie@bigc.edu.cn (Y.C.); huyingjie@njxzc.edu.cn (Y.H.); liluhai@bigc.edu.cn (L.L.)
† Joint first authors, these authors contributed equally.

Abstract: Herein, a simple approach for the fabrication of luminous self-assembled fibers based on halogen-bonded azopyridine complexes and oleic acid-modified quantum dots (QDs) is reported. The QDs uniformly align on the edge of the self-assembled fibers through the formation of van der Waals force between the alkyl chain of oleic acid on the QD surface and the alkyl chain of the halogen-bonded complexes, 15Br or 15I. Furthermore, the intermolecular interaction mechanism was elucidated by using Fourier-transform infrared spectroscopy (FTIR), Raman spectroscopy, and density functional theory (DFT) calculations. This approach results in retention of the fluorescence properties of the QDs in the fibers. In addition, the bromine-bonded fibers can be assembled into tailored directional fibers upon evaporation of the solvent (tetrahydrofuran) when using capillaries via the capillary force. Interestingly, the mesogenic properties of the halogen-bonded complexes are preserved in the easily prepared halogen-bonded fluorescent fibers; this provides new insight into the design of functional self-assembly materials.

Keywords: azopyridines; halogen bond; quantum dots; luminous self-assembled fibers

Citation: Pan, Y.; Xue, L.; Chen, Y.; Hu, Y.; Sun, Z.; Mo, L.; Li, L.; Yu, H. Luminous Self-Assembled Fibers of Azopyridines and Quantum Dots Enabled by Synergy of Halogen Bond and Alkyl Chain Interactions. *Molecules* **2022**, *27*, 8165. https://doi.org/10.3390/molecules27238165

Academic Editor: Marinella Striccoli

Received: 15 October 2022
Accepted: 15 November 2022
Published: 23 November 2022

1. Introduction

The design and synthesis of molecules that can self-assemble into functional supramolecular structures with fascinating properties through multiple noncovalent interactions is a frontier in the material and chemical research fields. Several organic self-assembled supramolecular functional fibers, which show promise for biomedical applications, have been synthesized via electrospinning and inter- or intramolecular interactions, resulting in well-defined morphologies [1–8]. The halogen bond, a versatile noncovalent interaction that has directionality, tunable interaction strength, good hydrophobicity, and is compatible with the large size of halogen atoms, has been used for the fabrication of supramolecular assemblies, such as photoresponsive mesogens [9], supramolecular gels [10–12], microphase structures [13], and photo-actuators [14]. However, its application to supramolecular functional fibers has been little explored. The first report of halogen-bonded fibers, published in 2013, involved the use of bis (pyridyl urea) and 1,4-diiodotetrafluorobenzene in polar media to achieve gelation [10]. Subsequently, the analogous halogen bond-based supramolecular sol-gel transition of azopyridines was reported; however, halogen-bonded fiber structures were not discussed [11,12].

Azopyridines, which exhibit interesting self-assembly and photoresponsive abilities, have been used to fabricate supramolecular assemblies and are regarded as the most widely used components in the field of supramolecular chemistry [15,16]. The majority of reported

azopyridine self-assembled fibers are constructed through hydrogen bonds and ionic bonds, and their self-assembly conditions and morphologies have been established. However, further investigation is required to develop supramolecular fibers with optical or electrical functions by mixing them with inorganic nanomaterial components. Quantum dots (QDs) are zero-dimensional inorganic materials with unique features, including high fluorescence efficiency, a narrow emission band, and tunable emission, owing to their size dependence; thus, they are commonly employed in solar cells, emitting diodes, biomedical imaging, and fluorescent anti-counterfeiting technology [17–25]. Recently, electrospun fluorescent fibers containing organic components and QD composites, such as CdSe/ZnS core-shell QDs and CdSe QDs, have been realized for use in polymeric lasers and optical sensors [26,27]. Furthermore, an intense circularly polarized luminescent material was prepared by forming a novel luminescent chiral nanotube using a chiral lipid gelator as a chiral template for the QDs [28]. However, the formation of azopyridine supramolecular fluorescent or directional fibers that incorporate inorganic nanomaterials through combined halogen bonds and van der Waals force has not yet been reported.

Considering this, we used our previously reported azopyridine halogen-bonded liquid crystal (LC) complexes (nX, X = Br, or I) to assemble fibers that exhibit an ordered orientation and luminescence (Scheme 1); details of the synthesis are presented in the ESI. We established that 15Br could promote the targeted directional arrangement of disordered supramolecular fibers with the aid of a capillary when tetrahydrofuran (THF) is used as a solvent. Mixing oleic acid-modified CdSe/ZnS core-shell QDs with the LC complexes resulted in the formation of large luminous fiber crystals of 15X@QDs (X = Br or I), in which the QDs were aligned along the edge of the self-assembled fibers due to van der Waals force between the long alkyl chain of oleic acid on the QD surface and 15Br or 15I. This is a novel approach for the fabrication of supramolecular structures with new properties and functions that can be applied in drug detection, biosensors, and electroluminescent devices.

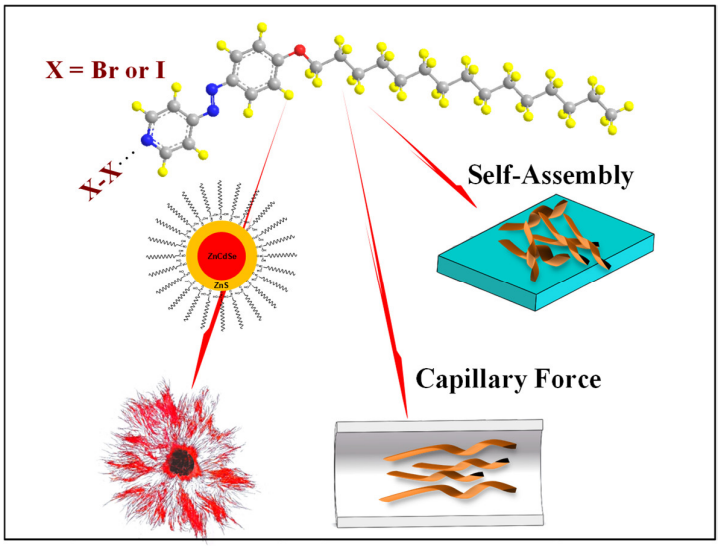

Scheme 1. Molecular structure of the used 15X (X = Br or I) and QDs, and the self-assembly process of the luminous fibers and directional fibers in the capillary in this work.

2. Results and Discussion

The halogen-bonded azopyridine fibers spontaneously formed either in the THF or upon the evaporation of one drop of the THF solution on the surface of the glass substrates in random order. The optical and scanning electron microscopy (SEM) images of the fibers (Figure 1a,b, respectively) reveal that the width of the supramolecular fibers of 15Br is on the micron scale. The effect of the alkyl chain length of the halogen-bonded complexes on the morphology of the fibers was investigated. Self-assembled fibers were formed in the THF using bromine-bonded complexes with alkyl chain lengths of 7 to 15 carbons

(Figure S2, ESI). The fibers of 15Br had a large aspect ratio, while the corresponding azopyridine derivatives did not form fibrous structures, which suggests that halogen bonds play a key role in facilitating the formation of supramolecular fibers.

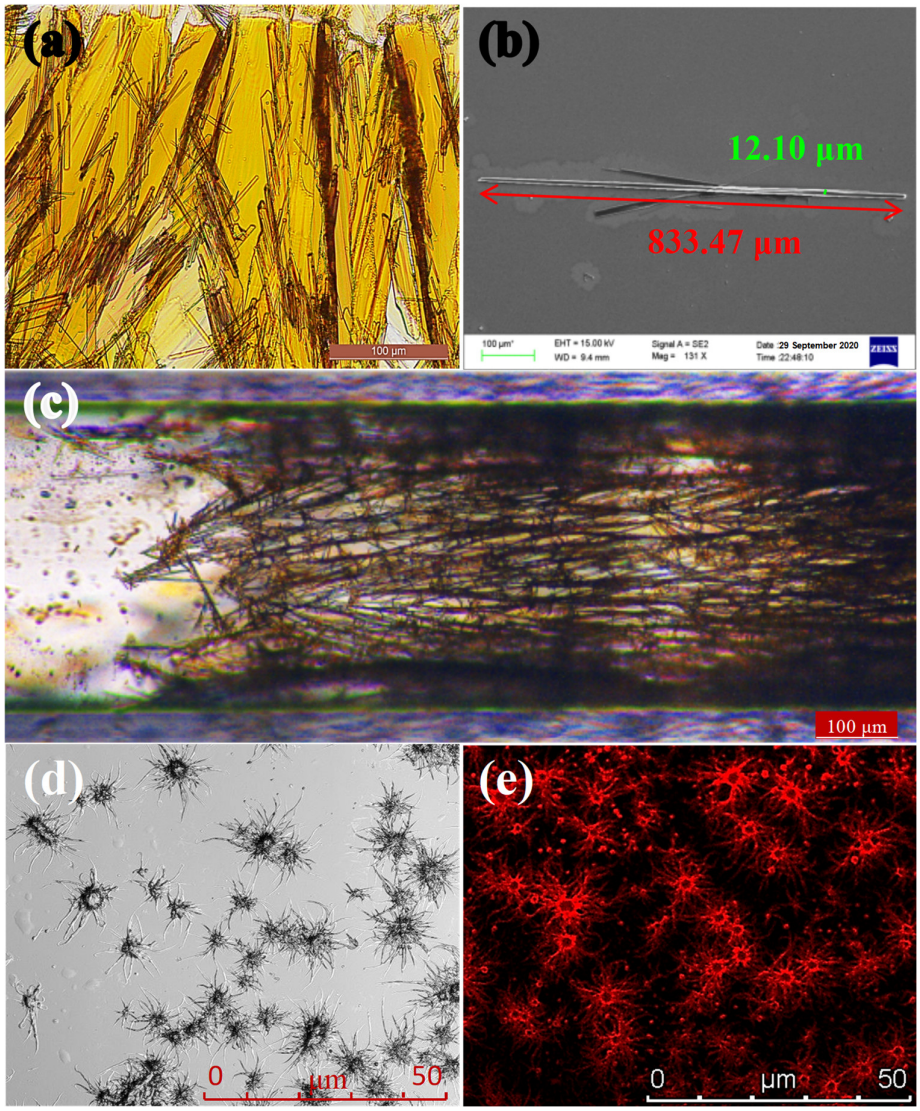

Figure 1. Optical (**a**) and SEM (**b**) images of 15Br fibers formed in the THF. Optical image (**c**) of 15Br formed directional fibers in the capillary after evaporation of the THF. Laser scanning confocal microscopy images of fluorescent fibers (**d**,**e**) from the 15Br@QDs mixture. Excitation source: λ_{ex} = 365 nm.

In addition, taking 15Br as a typical example, an increase in the mass concentration of 15Br in the THF from 0.1 to 1.0 wt% resulted in an increase in the number of visible self-assembled fibers (Figure S3, ESI). Subsequently, the morphologies of the fibers obtained from 15Br and its pristine counterpart, A15AzPy, were studied using six organic solvents with different polarity indices. The nature of the solvent influenced the morphology of the self-assembled fibers, indicating that the morphologies of the fabricated halogen-bonded fibers depended on the nature of the chosen organic solvent (Figures S4 and S5, ESI).

LCs are mesophasic, which means they exist between the melting and clearing points. Below its melting point, the material forms a normally ordered solid, and above the clearing point, it forms an isotropic liquid. The thermal properties of the self-assembled fibers fabricated by recrystallization of LC molecular 15Br were studied using differential scanning calorimetry (Figure S6a). The crystal-to-mesophase transition and the mesophase-

to-isotropic liquid transition temperatures increased significantly from 100.2 °C to 157.6 °C for the 15Br and 143.6 °C to 160.6 °C for the fibers, respectively. Moreover, the 15Br fibers have a narrower LC range than 15Br. In addition to obtaining optical microscopy images, the crystals of 15Br were purified in the THF and exhibited high melting and clearing points. These results were supported by the powder X-ray diffraction results (Figure S6b). Three diffraction peaks appear in the low-angle region for the 15Br fibers, similar to those observed for 15Br, and the *d*-spacing (1.78, 0.89, and 0.46 nm), which has a ratio of 1:1/2:1/4 and is consistent with a lamellar structure [29]. The peak at 1.78 nm, observed in the first-order reflection of the 15Br fibers, is sharp compared to the peak obtained for the pristine material, suggesting that the 15Br fibers are more ordered than those of the pristine material [30].

Moreover, 15Br could form directional self-assembled fibers in capillaries upon evaporation of the THF, owing to the capillary force [31–33], as shown in Figure 1c. This is a key technology in the development of high-performance organic materials.

Supramolecular luminescent fibers are particularly important because of their potential applications in interdisciplinary research, such as light-emitting electrochemical cells [34] and diagnostic devices [35,36]. The general method for the production of luminescent fibers involves electrospinning QDs in a polymer solution; however, this process has low production efficiency because the polymer solution has a slow rate of reaction, and the procedure is labor intensive [1]. In this study, novel luminescent halogen-bonded fibers were designed and easily obtained by mixing 15Br and oleic acid-modified CdSe/ZnS QDs in THF. As shown in Figure 1d,e the majority of the self-assembled fibers with bright fluorescence can be observed at the edges of the structures after the addition of QDs. The QDs supply fascinating luminescence properties without disturbing the fiber structures. Surface tension can cause the fluid to flow rapidly over the surface and remain almost stagnant in the internal area, while the QDs are carried to the edges by the Marangoni flow [37,38]. Furthermore, by increasing the volume-to-volume ratio of the QDs from 3:1 to 1:1, the aspect ratio of the self-assembled organic/inorganic hybrid composite (15Br@QDs) fibers can be increased, as shown by laser scanning confocal microscopy (Figure S7a–d). To eliminate the effects of the solvent used for the QDs on the morphology of the fibers, *n*-hexane and the QDs in *n*-hexane were added separately to the THF solution of 15Br, using the same ratio as used previously, and analyzed by SEM and energy-dispersive X-ray spectroscopy (EDS). The mixture of 15Br in THF and the oleic acid-modified CdSe/ZnS QDs in *n*-hexane spontaneously self-assembled into fibers with a high aspect ratio (Figure S8a), while inhomogeneous structures self-assembled upon the addition of *n*-hexane to 15Br in the absence of QDs (Figure S8b). The EDS results indicate that QDs were present on the fibers of the 15Br@QDs (Figure S8c,d), which contributed to the formation of large-aspect-ratio self-assembled luminous fibers. In addition, A15AzPy@QDs could also form self-assembled fibers due to the van der Waals interactions between alkyl chains (Figure S9). The fluorescence properties of 15Br@QDs in solution are shown in Figure 2a. The emission peaks of CdSe/ZnS QDs exhibited a similar pattern to those of the resultant fibers, while being slightly red-shifted, indicating the conservation of the fundamental fluorescence properties of the QD-assisted luminescent fibers.

Raman spectroscopy is a powerful tool for investigating halogen bonds [39,40]. As shown in Figure 2b, the Br–Br stretching peaks of the 15Br fibers shifted to a lower wavenumber relative to those of 15Br (219.7 cm^{-1} to 207.2 cm^{-1}), which indicates not only that the 15Br fibers are halogen bonded, but also that the recrystallization of the 15Br fibers from 15Br in THF weakens the halogen bond and leads to a decrease in the Br–Br vibration frequency of the 15Br fibers. Furthermore, the Br–Br stretching vibration peaks of 15Br@QDs observed at 216.8 cm^{-1}, suggest that the weak van der Waals force between alkyl chains has a subtle influence on the halogen bond. This suggests that the halogen bond plays a major role in the self-assembly of the azopyridine fibers, and the QDs further aid the self-assembly process via van der Waals force, leading to the formation of luminous fibers.

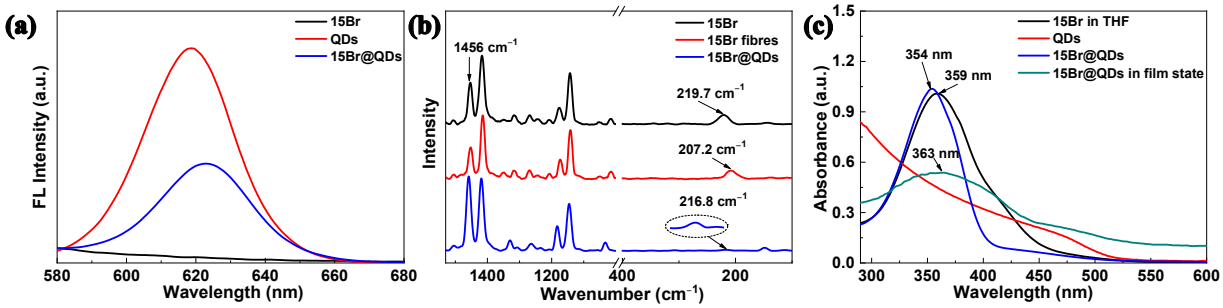

Figure 2. (**a**) Fluorescence spectra of 15Br in THF (0.4 wt%), QDs in *n*−hexane and 15Br@QDs mixture (V_{15Br}/V_{QDs} = 1:1). (**b**) Raman spectra of 15Br, 15Br fibers and 15Br@QDs in solid. (**c**) UV−vis absorption spectra of 15Br in THF, QDs and 15Br@QDs in different states.

Figure 2c shows the UV-vis absorption spectra of 15Br in the THF, CdSe/ZnS QDs, 15Br@QDs solution, and 15Br@QDs film. The maximum absorption of 15Br and 15Br@QDs in THF occurs at wavelengths of 359 and 354 nm, respectively, which is attributable to the azobenzene π–π * bands. The spectrum of 15Br@QDs reveals a small blue shift relative to the 15Br spectrum, which is caused by the substituent effect of the carboxylate groups of oleic acid on the surface of the QDs and bromine atom. In contrast, the peak at 363 nm in the spectrum of 15Br@QDs in solution was red-shifted in the spectrum of the 15Br@QDs film. This red shift may be attributable to the *J*-aggregation of the chromophores, which are partly arranged in close proximity to each other and with coplanar transition dipoles [41–47].

The distribution of CdSe/ZnS QDs in the halogen-bonded fibers was observed using transmission electron microscopy (Figure 3). Interestingly, the 15Br fibers can act as a template for the arrangement of QDs during self-assembly. Thus, the CdSe/ZnS QDs were uniformly distributed along the edge of the halogen-bonded fibers owing to the van der Waals force between 15Br and the QDs, resulting in the preservation of the original fluorescence properties of the QDs, as confirmed by the absorption and fluorescence spectral data. In addition, the EDS maps of the fibers indicate the presence and even distribution of Br, S, Cd, Se, and Zn in the QDs on the fibers (Figure 3c–g). The introduction of long-alkyl-chain-functionalized QDs promotes interactions between the QDs and halogen-bonded complexes, resulting in luminous fibers.

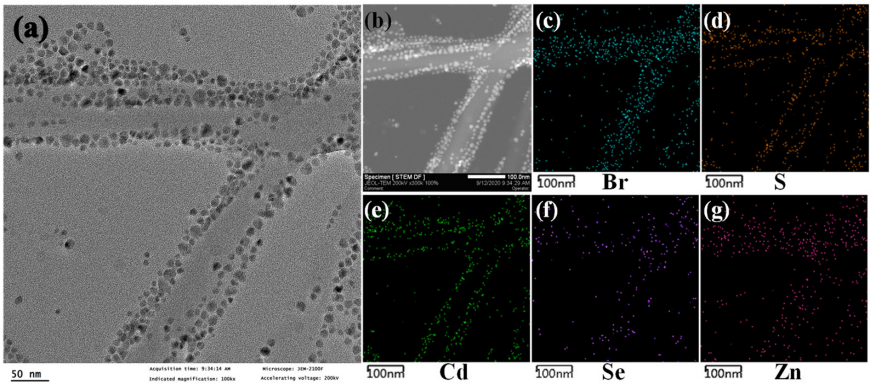

Figure 3. TEM image (**a**) and STEM image (**b**) of 15Br@QDs fibers. EDS Br and QDs elemental mapping images (**c**–**g**). Mapping of the Br region is depicted in blue; S is orange; Cd is green; Se is purple; and the Zn region is shown in pink.

Furthermore, the LC properties of the 15Br@QDs were determined using polarizing optical microscopy; 15Br@QDs were shown to have a focal conical fan texture similar to that of 15Br (Figure S10). Moreover, the aligned 15Br@QDs mesogens show strong anisotropy in their polarized UV-vis absorption spectra, and the orientation factor (0.052) compares favorably with that of pristine 15Br (0.004) (Figure S11).

To evaluate the bonding capability of the AzPy derivatives and QDs as a function of the halogen atom, molecular iodine was used as a Lewis base instead of molecular bromine for the preparation of iodine-bonded 15I@QDs complexes. The aspect ratio of the self-assembled luminous 15I@QD fibers is expected to be large compared to that of the 15Br@QDs owing to the presence of the QDs (Figure 4a,b). This could be because the halogen bonds decrease in strength in the following order: I > Br > Cl [48–51], and the relatively weak bromine bonds led to a reduction in the aspect ratios. The standard deviations of the aspect ratios of the 15Br, 15Br@QDs, and 15I@QDs fibers are calculated in the ESI.

Considering the photoresponsivity of our prototype molecule 15I, the photoactivity of the 15I@QDs was monitored before and after UV irradiation at 360 nm in the THF solution. Exposure of the 15I@QD solution to UV light resulted in a gradual decrease in the absorption peak at 358 nm, which can be attributed to a π–π * transition, and a gradual increase in the peak at 442 nm, which can be attributed to the n–π * transition (Figure 4c). This is the result of photoisomerization of AzPy molecules from their *trans* to *cis* isomers. The intensity of the absorption peak at 358 nm gradually increased, and that at 442 nm decreased when the irradiated sample was kept in the dark, indicating that the 15I@QDs underwent trans to cis to trans isomerization (Figure 4d). However, this photochemical phase transition was not observed for 15Br@QDs, which produced a spectrum analogous to that of the brominated 15Br compound when irradiated with UV light.

Density functional theory (DFT), specifically the Gaussian 16 program, was used to investigate possible 15X@QDs (X = Br or I) interactions [52]. Geometry optimization calculations were performed using the B3LYP DFT-D3 method [53–55], and the 6−311G + (2d,2p) basis set was used to locate all stationary points involved. The vibrational frequencies were computed at the same level of theory to check whether each optimized structure is an energy minimum or transition state and to evaluate its zero-point energy. The binding energy (E_b) is defined as $E_b = E_{A+B}$—($E_A + E_B$), where E_{A+B} is the total energy of A and B combined, and $E_A + E_B$ is the sum of the total energies of A and B before the combination. A and B refer to 15X and alkyl chains of oleic acid on the QD surface, respectively.

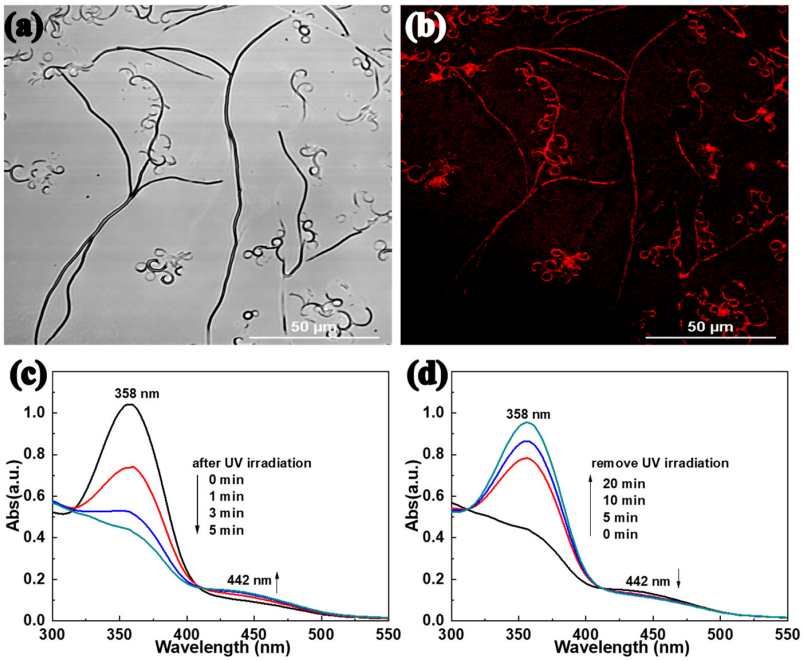

Figure 4. (**a**,**b**) Laser scanning confocal microscopy images of fluorescent fibers from 15I@QDs mixture. Excitation source: λ_{ex} = 365 nm. (**c**,**d**) UV-vis absorption spectra of 15I@QDs in the THF solution after UV irradiation and relaxed in the dark immediately after UV irradiation.

The E_b energies of 15Br@QDs with 4, 8, 15 overlap of alkyl chains via van der Waals force were calculated to be −0.15125 eV, −0.30105 eV and −0.52469 eV, respectively, and the E_b of 15I@QDs were calculated to be −0.15254 eV, −0.30102 eV and −0.52463 eV, respectively (Figure 5). The energy analysis shows that the absolute value of binding energy of 15X@QDs is getting bigger and bigger as the overlap of alkyl chains increases between QDs and 15X molecules via van der Waals force, which led to the further stabilization of the entire system of 15X@QDs.

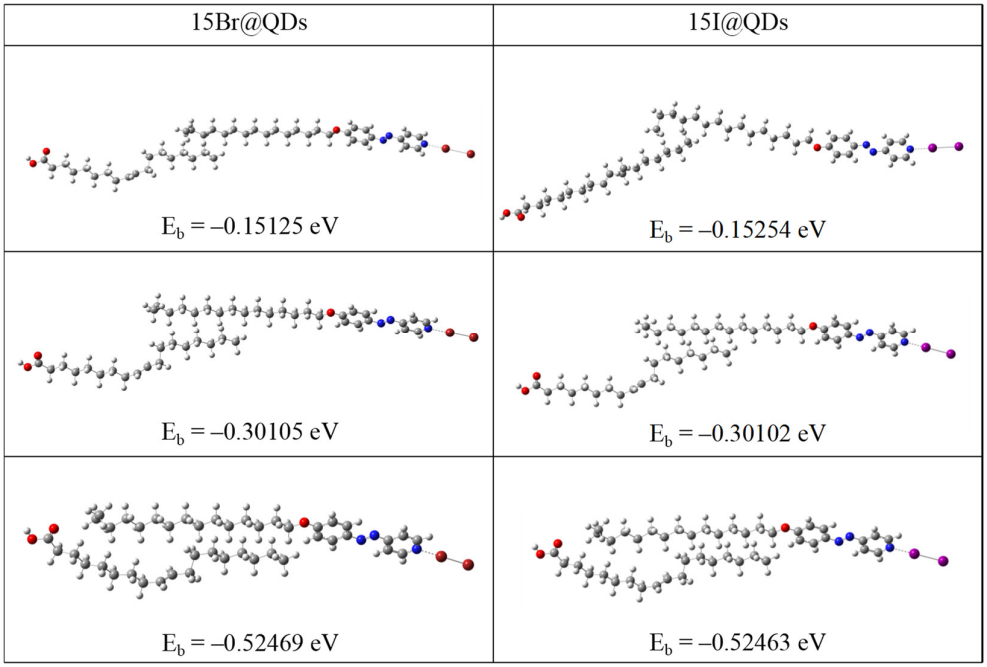

Figure 5. DFT optimized structures of 15X@QDs (X = Br or I).

3. Materials and Methods

Materials: 4-aminopyridine, K_2CO_3, acetone and other chemical reagents were obtained from Sigma-Aldrich, Saint Louis, MO, USA. CdSe/ZnS QDs were purchased from Wuhan Jiayuan Quantum Dot Co., Ltd. Wuhan, China. The maximum emission wavelength is 625 nm ± 5 nm, and the size is 5–10 nm. The specification is 30 mg powder QDs dispersed in 10 mL *n*-hexane solvent.

Characterizations: ^{1}H NMR spectra were executed on a Bruker Avance III 400. Differential scanning calorimetry (DSC) examination was performed on a Perkin-Elmer DSC 8000 with a heating and cooling rate of 10 °C/min. The morphologies of fibers were observed using scanning electron microscopy (SEM, Zeiss EVO18, Oberkochen, BW, Germany), polarizing optical microscope (POM, LEICA DM2700 M, Wetzlar, Hesse, Germany) and transmission electron microscopy (TEM, Tecnai G2 F20, Hillsboro, OR, USA). The powder X-ray diffraction analysis (XRD) was implemented on a Philips X pert pro. The FT-IR analysis and the UV-vis analysis were measured using Nicolet 510P IR spectra and a UV/VIS/NIR spectrometer (Perkin-Elmer lambda 950, Waltham, MA, USA). Laser scanning confocal microscopy was recorded on the Zeiss LSM800.

Simulation method: All calculations were performed using the Gaussian 16 program. Geometry optimization calculations were performed using the B3LYP DFT-D3 method.

4. Conclusions

In conclusion, we report that the self-assembled fibers can be developed from halogen-bonded complexes by varying the alkyl-chain lengths, concentrations, and solvents. We found that 15Br, with the aid of a capillary, can form directional self-assembly fibers in THF. Interestingly, the self-assembled luminous fibers were obtained by the synergy interactions

of halogen bonds and van der Waals force between the oleic acid groups of the QDs surface and the alkyl chain of the halogen-bonded complexes, which is critical to potential applications, such as drug detection, biosensors, electroluminescent devices, and other novel optical devices.

Supplementary Materials: The following are available online at https://www.mdpi.com/article/10.3390/molecules27238165/s1, Scheme S1. Synthesis of the 15X@QDs; Figure S1. ^{1}H NMR spectrum of the A15AzPy (compound a2); Figure S2. Optical images of bromine–bonded fibres with different alkyl chains formed in THF; Figure S3. The picture of different mass concentration of 15Br from 0.1 to 1.0 wt% in THF; Figure S4. Optical and SEM images of the self-assembled fibres formed from 15Br (0.4 wt%) in different organic solvents at room temperature. (a) dichloromethane (DCM), (c) tetrahydrofuran (THF), (e) ethanol, (g) acetone, (i) N,N–dimethylformamide (DMF), (k) methanol and (m) dimethylsulfoxide (DMSO) are optical images, (b, d, f, h, j, l, n) are SEM images; Figure S5. Optical and SEM images of A15AzPy with 0.4 wt% mass concentration obtained in different solvents at room temperature. (a) dichloromethane (DCM), (c) tetrahydrofuran (THF), (e) ethanol, (g) N,N–dimethylformamide (DMF), (i) methanol and (k) dimethylsulfoxide (DMSO) are optical images, (b, d, f, h, j, l) are SEM images; Figure S6.The DSC measurements (a), XRD patterns (b) of 15Br and 15Br fibres at room temperature; Figure S7. Laser scanning confocal microscopy images of 15Br@QDs from the mixtures of 15Br (0.4 wt%) in THF and CdSe/ZnS QDs in *n*-hexane. The volume ratio of 15Br and QDs are (a) 3:1, (b) 2:1, (c) 1.5:1, (d) 1:1; Figure S8. SEM images of 15Br (0.4 wt%) in THF (a) adding QDs, (b) adding *n*-hexane mixed solvent, (c) and (d) are their EDS images; Figure S9. Optical images of the self-assembled fibres formed from A15AzPy@QDs (volume-to-volume ratio = 3:1) in THF at different temperature. Figure S10. POM pictures of 15Br (a) and 15Br@QDs (b); Figure S11. Polarized UV−Vis spectra of 15Br@QD (a) and 15Br (b) films. The black and red curves are the absorption parallel and perpendicular to the orientation direction, respectively.

Author Contributions: Conceptualization, Y.P.; methodology, Y.C. and H.Y.; software, Y.H.; validation, H.Y. and L.L.; formal analysis, Y.C., Y.H. and H.Y.; investigation, L.X. and Y.P.; resources, Y.C., L.L., L.M. and Z.S.; data curation, Y.P. and L.X.; writing—original draft preparation, Y.P.; writing—review and editing, Y.P. and L.X.; visualization, Y.C., Y.H. and H.Y.; supervision, Y.C. and H.Y.; project administration, L.L., Y.H. and H.Y.; funding acquisition, Y.C., L.L., L.M. and Z.S. All authors have read and agreed to the published version of the manuscript.

Funding: This work was supported by the National Natural Science Foundation of China (Grant No. s 51927806, 51773002), Science and Technology Planning Project of 2020 Beijing Education Commission (KM202010015006), Beijing Municipal Natural Science Foundation (No. 2192017), National Key R&D Program of China (2018YFB0703702), R&D Plan of Beijing Institute of Graphic Communication (Ec202005), Natural Science Foundation of Jiangsu (BK20201120) and Excellent Science and Technology Innovation Group of Jiangsu Province.

Institutional Review Board Statement: Not applicable.

Informed Consent Statement: Not applicable.

Data Availability Statement: Not applicable.

Conflicts of Interest: The authors declare no conflict of interest.

Sample Availability: Samples of the compounds are available from the authors.

References

1. Li, D.; Xia, Y. Electrospinning of nanofibers: Reinventing the wheel? *Adv. Mater.* **2004**, *16*, 1151–1170. [CrossRef]
2. Lu, X.; Zhao, Y.; Wang, C. Fabrication of PbS nanoparticles in polymer-fiber matrices by electrospinning. *Adv. Mater.* **2005**, *17*, 2485–2488. [CrossRef]
3. Lu, X.; Zhao, Y.; Wang, C.; Wei, Y. Fabrication of Cds nanorods in PVP fiber matrices by electrospinning. *Macromol. Rapid Commun.* **2005**, *26*, 1325–1329. [CrossRef]
4. Son, W.K.; Cho, D.; Park, W.H. Direct electrospinning of ultrafine titania fibres in the absence of polymer additives and formation of pure anatase titania fibres at low temperature. *Nanotechnology.* **2005**, *17*, 439–443. [CrossRef]
5. Aoki, K.; Nakagawa, M.; Ichimura, K. Self-assembly of amphoteric azopyridine carboxylic acids: Organized structures and macroscopic organized morphology influenced by heat, pH change, and light. *J. Am. Chem. Soc.* **2000**, *122*, 10997–11004. [CrossRef]

6. Nakagawa, M.; Ishii, D.; Aoki, K.; Seki, T.; Iyoda, T. Tubular and twisted Ni–P fibers molded from morphology-tunable and recyclable organic templates of hydrogen-bonded supramolecular assemblages. *Adv. Mater.* **2005**, *17*, 200–205. [CrossRef]
7. Pasini, D.; Kraft, A. Supramolecular self-assembly of fibres. *Curr. Opin. Solid State Mater. Sci.* **2004**, *8*, 157–163. [CrossRef]
8. Wu, Y.; Shah, D.U.; Liu, C.; Yu, Z.; Liu, J.; Ren, X.; Rowland, M.J.; Abell, C.; Ramage, M.H.; Scherman, O.A. Bioinspired supramolecular fibers drawn from a multiphase self-assembled hydrogel. *Proc. Natl. Acad. Sci. USA* **2017**, *114*, 8163–8168. [CrossRef]
9. Chen, Y.; Yu, H.; Zhang, L.; Yang, H.; Lu, Y. Photoresponsive liquid crystals based on halogen bonding of azopyridines. *Chem. Commun.* **2014**, *50*, 9647–9649. [CrossRef]
10. Meazza, L.; Foster, J.A.; Fucke, K.; Metrangolo, P.; Resnati, G.; Steed, J.W. Halogen-bonding-triggered supramolecular gel formation. *Nat. Chem.* **2013**, *5*, 42–47. [CrossRef]
11. Hu, H.; Qiu, Y.; Wang, J.; Zhao, D.; Wang, H.; Wang, Q.; Liao, Y.; Peng, H.; Xie, X. Photomodulated morphologies in halogen bond–driven assembly during gel–sol transition. *Macromol. Rapid Commun.* **2019**, *40*, 1800629. [CrossRef] [PubMed]
12. Tong, X.; Qiu, Y.; Zhao, X.; Xiong, B.; Liao, R.; Peng, H.; Liao, Y.; Xie, X. Visible light-triggered gel-to-sol transition in halogen-bond-based supramolecules. *Soft Matter* **2019**, *15*, 6411–6417. [CrossRef] [PubMed]
13. Chen, Y.; Huang, S.; Wang, T.; Yu, H. Enhanced ordering and efficient photoalignment of nanostructures in block copolymers enabled by halogen bond. *Macromolecules* **2020**, *53*, 1486–1493. [CrossRef]
14. Li, X.; Ma, S.; Hu, J.; Ni, Y.; Lin, Z.; Yu, H. Photo-activated bimorph composites of kapton and liquid-crystalline polymer towards biomimetic circadian rhythms of albizia julibrissin leaves. *J. Mater. Chem. C* **2019**, *7*, 622–629. [CrossRef]
15. Chen, Y.; Quan, M.; Yu, H.; Zhang, L.; Yang, H.; Lu, Y. Fabrication of nanofibres with azopyridine compounds in various acids and solvents. *RSC Adv.* **2015**, *5*, 31219–31225. [CrossRef]
16. El Malah, T.; Nour, H.F. Click synthesis of shape-persistent azodendrimers and their orthogonal self-assembly to nanofibres. *Aust. J. Chem.* **2018**, *71*, 463–472. [CrossRef]
17. Shirasaki, Y.; Supran, G.J.; Bawendi, M.G.; Bulović, V. Emergence of colloidal quantum-dot light-emitting technologies. *Nat. Photonics* **2013**, *7*, 13–23. [CrossRef]
18. Jiang, C.; Zhong, Z.; Liu, B.; He, Z.; Zou, J.; Wang, L.; Wang, J.; Peng, J.; Cao, Y. Coffee-ring-free quantum dot thin film using inkjet printing from a mixed-solvent system on modified ZnO transport layer for light-emitting devices. *ACS Appl. Mater. Interfaces* **2016**, *8*, 26162–26168. [CrossRef] [PubMed]
19. Anikeeva, P.O.; Halpert, J.E.; Bawendi, M.G.; Bulović, V. Quantum dot light-emitting devices with electroluminescence tunable over the entire visible spectrum. *Nano Lett.* **2009**, *9*, 2532–2536. [CrossRef]
20. Pattantyus-Abraham, A.G.; Kramer, I.J.; Barkhouse, A.R.; Wang, X.; Konstantatos, G.; Debnath, R.; Levina, L.; Raabe, I.; Nazeeruddin, M.K.; Grätzel, M.; et al. Depleted-heterojunction colloidal quantum dot solar cells. *ACS Nano.* **2010**, *4*, 3374–3380. [CrossRef] [PubMed]
21. Kim, B.H.; Onses, M.S.; Lim, J.B.; Nam, S.; Oh, N.; Kim, H.; Yu, K.J.; Lee, J.W.; Kim, J.-H.; Kang, S.-K.; et al. High-resolution patterns of quantum dots formed by electrohydrodynamic jet printing for light-emitting diodes. *Nano Lett.* **2015**, *15*, 969–973. [CrossRef] [PubMed]
22. Vu, T.Q.; Lam, W.Y.; Hatch, E.W.; Lidke, D.S. Quantum dots for quantitative imaging: From single molecules to tissue. *Cell Tissue Res.* **2015**, *360*, 71–86. [CrossRef] [PubMed]
23. Valizadeh, A.; Mikaeili, H.; Samiei, M.; Farkhani, S.M.; Zarghami, N.; Kouhi, M.; Akbarzadeh, A.; Davaran, S. Quantum dots: Synthesis, bioapplications, and toxicity. *Nanoscale Res. Lett.* **2012**, *7*, 480. [CrossRef] [PubMed]
24. Sun, L.-W.; Shi, H.-Q.; Li, W.-N.; Xiao, H.-M.; Fu, S.-Y.; Cao, X.-Z.; Li, Z.-X. Lanthanum-doped ZnO quantum dots with greatly enhanced fluorescent quantum yield. *J. Mater. Chem.* **2012**, *22*, 8221–8227. [CrossRef]
25. Han, T.; Yuan, Y.; Liang, X.; Zhang, Y.; Xiong, C.; Dong, L. Colloidal stable quantum dots modified by dual functional group polymers for inkjet printing. *J. Mater. Chem. C* **2017**, *5*, 4629–4635. [CrossRef]
26. Abitbol, T.; Wilson, J.T.; Gray, D.G. Electrospinning of fluorescent fibers from CdSe/ZnS quantum dots in cellulose triacetate. *J. Appl. Polym. Sci.* **2011**, *119*, 803–810. [CrossRef]
27. He, X.; Tan, L.; Wu, X.; Yan, C.; Chen, D.; Meng, X.; Tang, F. Electrospun quantum dots/polymer composite porous fibers for turn-on fluorescent detection of lactate dehydrogenase. *J. Mater. Chem.* **2012**, *22*, 18471–18478. [CrossRef]
28. Huo, S.; Duan, P.; Jiao, T.; Peng, Q.; Liu, M. Self-assembled luminescent quantum dots to generate full-color and white circularly polarized light. *Angew. Chem. Int. Ed.* **2017**, *56*, 12174–12178. [CrossRef]
29. Duan, P.; Li, Y.; Li, L.; Deng, J.; Liu, M. Multiresponsive chiroptical switch of an azobenzene-containing lipid: Solvent, temperature, and photoregulated supramolecular chirality. *J. Phys. Chem. B.* **2011**, *115*, 3322–3329. [CrossRef]
30. Draper, M.; Saez, I.M.; Cowling, S.J.; Gai, P.; Heinrich, B.; Donnio, B.; Guillon, D.; Goodby, J.W. Self-assembly and shape morphology of liquid crystalline gold metamaterials. *Adv. Funct. Mater.* **2011**, *21*, 1260–1278. [CrossRef]
31. Duan, H.; Berggren, K.K. Directed self-assembly at the 10 nm scale by using capillary force-induced nanocohesion. *Nano Lett.* **2010**, *10*, 3710–3716. [CrossRef] [PubMed]
32. Kim, S.M.; Kim, J.; Kang, S.M.; Jang, S.; Kang, D.; Moon, S.E.; Kim, H.N.; Yoon, H. Directional clustering of slanted nanopillars by elastocapillarity. *Small* **2016**, *12*, 3764–3769. [CrossRef]
33. Zhao, S.; Wu, Y.; Lu, W.; Liu, B. Capillary force driving directional 1D assembly of patchy colloidal discs. *ACS Macro Lett.* **2019**, *8*, 363–367. [CrossRef] [PubMed]

34. Zhang, Z.; Guo, K.; Li, Y.; Guan, G.; Li, H.; Luo, Y.; Zhao, F.; Zhang, Q.; Pei, Q.; Peng, H. A colour-tunable, weavable fibre-shaped polymer light-emitting electrochemical cell. *Nat. Photonics* **2015**, *9*, 233–238. [CrossRef]
35. Wang, Y.; Jin, Y.; Zhang, T.; Huang, Z.; Yang, H.; Wang, J.; Jiang, K.; Fan, S.; Li, Q. Emission enhancement from CdSe/ZnS quantum dots induced by strong localized surface plasmonic resonances without damping. *J. Phys. Chem. Lett.* **2019**, *10*, 2113–2120. [CrossRef]
36. Bhaskar, S.; Singh, A.K.; Das, P.; Jana, P.; Kanvah, S.; Bhaktha, S.; Ramamurthy, S.S. Superior resonant nanocavities engineering on the photonic crystal-coupled emission platform for the detection of femtomolar iodide and zeptomolar cortisol. *ACS Appl. Mater. Interfaces* **2020**, *12*, 34323–34336. [CrossRef] [PubMed]
37. Liu, D.; Broer, D.J. New insights into photoactivated volume generation boost surface morphing in liquid crystal coatings. *Nat. commun.* **2015**, *6*, 8334. [CrossRef]
38. Cai, Z.; Huang, Z.; Li, Z.; Su, M.; Zhao, Z.; Qin, F.; Zhang, Z.; Yang, J.; Song, Y. Evaporation induced spontaneous micro-vortexes through engineering of the Marangoni flow. *Angew. Chem. Int. Ed.* **2020**, *132*, 23892–23897. [CrossRef]
39. Erdélyi, M. Halogen bonding in solution. *Chem. Soc. Rev.* **2012**, *41*, 3547–3557. [CrossRef] [PubMed]
40. Pang, X.; Wang, H.; Zhao, X.R.; Jin, W.J. Anionic 3d cage networks self-assembled by iodine and v-shaped pentaiodides using dimeric oxoammonium cations produced in situ as templates. *Dalton Trans.* **2013**, *42*, 8788–8795. [CrossRef]
41. Menzel, H.; Weichart, B.; Schmidt, A.; Paul, S.; Knoll, W.; Stumpe, J.; Fischer, T. Small-angle X-ray scattering and ultraviolet-visible spectroscopy studies on the structure and structural changes in langmuir-blodgett films of polyglutamates with azobenzene moieties tethered by alkyl spacers of different length. *Langmuir* **1994**, *10*, 1926–1933. [CrossRef]
42. Ren, H.; Chen, D.; Shi, Y.; Yu, H.; Fu, Z. A carboxylic azo monomer and its homopolymer: Synthesis, self-organization and fluorescence behaviour in solution. *Polym. Chem.* **2015**, *6*, 270–277. [CrossRef]
43. Kunitake, T. Synthetic bilayer membranes: Molecular design, self-organization, and application. *Angew. Chem. Int. Ed.* **1992**, *31*, 709–726. [CrossRef]
44. Han, M.; Ichimura, K. In-plane and tilt reorientation of p-methoxyazobenzene side chains tethered to liquid crystalline polymethacrylates by irradiation with 365 nm light. *Macromolecules* **2001**, *34*, 90–98. [CrossRef]
45. Tong, X.; Cui, L.; Zhao, Y. Confinement effects on photoalignment, photochemical phase transition, and thermochromic behavior of liquid crystalline azobenzene-containing diblock copolymers. *Macromolecules* **2004**, *37*, 3101–3112. [CrossRef]
46. Kasha, M.; Rawls, H.R.; El-Bayoumi, M.A. The exciton model in molecular spectroscopy. *Pure Appl. Chem.* **1965**, *11*, 371–392. [CrossRef]
47. Wu, S.; Niu, L.; Shen, J.; Zhang, Q.; Bubeck, C. Aggregation-induced reversible thermochromism of novel azo chromophore-functionalized polydiacetylene cylindrical micelles. *Macromolecules* **2009**, *42*, 362–367. [CrossRef]
48. Nguyen, H.L.; Horton, P.N.; Hursthouse, M.B.; Legon, A.C.; Bruce, W.D. Halogen bonding: A new interaction for liquid crystal formation. *J. Am. Chem. Soc.* **2004**, *126*, 16–17. [CrossRef]
49. McAllister, L.J.; Präsang, C.; Wong, J.P.W.; Thatcher, R.J. Halogen-bonded liquid crystals of 4-alkoxystilbazoles with molecular iodine: A very short halogen bond and unusual mesophase stability. *Chem. Commun.* **2013**, *49*, 3946–3948. [CrossRef]
50. Stammreich, H.; Forneris, R.; Tavares, Y. High-resolution Raman spectroscopy in the red and near infrared—II: Vibrational frequencies and molecular interactions of halogens and diatomic interhalogens. *Spectrochim. Acta* **1961**, *17*, 1173–1184. [CrossRef]
51. Klaeboe, P. The Raman spectra of some iodine, bromine, and iodine monochloride charge-transfer coomplexes in solution. *J. Am. Chem. Soc.* **1967**, *89*, 3667–3676. [CrossRef]
52. Frisch, M.J.; Trucks, G.W.; Schlegel, H.B.; Scuseria, G.E.; Robb, M.A.; Cheeseman, J.R.; Scalmani, G.; Barone, V.; Petersson, G.A.; Nakatsuji, H.; et al. *Gaussian 16 Rev. C.01*; Guassian Inc.: Wallingford, CT, USA, 2016.
53. Parr, R.G.; Yang, W. *Density-Functional Theory of Atoms and Molecules*, 1st ed.; Oxford University Press, Inc.: New York, NY, USA, 1989.
54. Lee, C.; Yang, W.; Parr, R.G. Development of the Colle-Salvetti correlation-energy formula into a functional of the electron density. *Phys. Rev. B* **1988**, *37*, 785–789. [CrossRef] [PubMed]
55. Becke, A.D. Density-functional thermochemistry. III. The role of exact exchange. *J. Chem. Phys.* **1993**, *98*, 5648–5652. [CrossRef]